Oxygen-stabilized triangular defects in hexagonal boron nitride

S. P. Huber, E. Gullikson, R. W. E. van de Kruijs, F. Bijkerk, and D. Prendergast

Phys. Rev. B **92**, 245310 — Published 29 December 2015

DOI: 10.1103/PhysRevB.92.245310

Oxygen stabilized triangular defects in hexagonal boron nitride

S. P. Huber,[1, 2, *] E. Gullikson,[3] R. W. E. van de Kruijs,[2] F. Bijkerk,[2] and D. Prendergast[1]

[1] *Molecular Foundry, Lawrence Berkeley National Laboratory, Berkeley, California 94720, United States*
[2] *Industrial Focus Group XUV Optics, MESA + Research Institute for Nanotechnology, University of Twente, P.O. Box 217, 7500 AE, Enschede, The Netherlands*
[3] *Center for X-Ray Optics, Lawrence Berkeley National Laboratory, Berkeley, California 94720, United States*

Recently several experimental transmission electron microscopy (TEM) studies have reported the observation of nanoscale triangular defects in mono- and multilayer hexagonal boron nitride (h-BN). First-principles calculations are employed to study the thermodynamical stability and spectroscopic properties of these triangular defects and the chemical nature of their edge termination. Oxygen terminated defects are found to be significantly more stable than defects with nitrogen terminated edges. Simulated x-ray absorption spectra of the boron K-edge for oxygen terminated defects show excellent agreement with experimental x-ray absorption near-edge spectroscopy (XANES) measurements on defective h-BN films with oxygen impurities. Finally we show that the structural model for oxygen defects in h-BN as deduced from the simulated core level spectroscopy is intrinsically linked to the equilateral triangle shape of defects as observed in many recent electron microscopy measurements.

PACS numbers: 31.15.A-, 78.70.Dm, 78.40.-q, 73.22.-f

Hexagonal boron nitride (h-BN) is an sp^2-bonded planar material and an isoelectronic structural analogue of graphite with very similar lattice parameters. Like its carbon-based counterpart, h-BN has many interesting properties such as high in-plane mechanical strength and thermal conductivity[1,2] and has been shown to have an even higher chemical stability compared to graphite[3]. Despite the many structural similarities between h-BN and graphite however, there are also significant differences in material properties. Unlike the semimetal graphite, h-BN is a wide gap insulator[4] which allows it to be used as an ultraviolet emitter in optoelectronics[5]. Recently monolayer boron nitride g-BN has been successfully synthesized[6] and makes a great candidate for use in conjunction with graphene in novel electronics due to their structural commensurability but contrasting electronic properties[7].

A high degree of structural quality and integrity is crucial for these applications[8], however, recently several studies on structural defects in h-BN have been published[9–12] that observe the formation of voids of various sizes with a very distinctive equilateral triangular shape. The methods employed to study these triangular structural imperfections and their formation are electron microscopy based techniques such as annular dark field (ADF) imaging and transmission electron microscopy (TEM). The high spatial resolution of these techniques allows for a very accurate analysis of the structural and geometrical properties of the observed defects, but the marginal chemical sensitivity limits the capabilities to study chemical properties, specifically of the atoms located at the edge of the void created by the defects. In an effort to gain more insight into the chemical nature of the defects and their edge termination, recent studies have conducted STEM-EELS measurements to elucidate the spectroscopic signature of triangular voids at the nitrogen[12] and boron K-edge[13]. The results show very characteristic features in the respective core-level spectra and indicate that spectroscopic methods are ideal candidates to investigate the true chemical nature of triangular defects in h-BN, which is still open to debate.

The early TEM studies report almost exclusively boron centric vacancies with nitrogen terminated edges, as confirmed by the STEM-EELS work of Suenaga[12], with the origin of this asymmetry being attributed to the lower knock-on threshold value of boron compared to that of nitrogen under influence of the electron beam of the TEM measurement itself[14], while nitrogen centric vacancies have since also been shown to exist under certain experimental conditions[13]. In stark contrast, X-ray Absorption Near Edge Spectroscopy (XANES) studies on defective h-BN thin films have exclusively observed nitrogen voids[15] or oxygen impurity defects[16–18] as indicated by very prominent and distinguishing features in the boron K-edge spectrum. In this work we provide a solution for this apparent contradiction in literature by means of theoretical calculations from first-principles on the thermodynamic stability, chemical nature and spectroscopic properties of triangular defects that apply to both bulk and monolayer h-BN. Our results reveal a direct link between the geometric properties of the experimentally observed vacancy based defects and distinctive spectral features observed in core-level spectroscopy measurements.

I. COMPUTATIONAL METHOD

A. Structural relaxation and molecular dynamics

All structural optimizations and molecular dynamics have been carried out within the DFT framework using the Vienna *ab initio* simulation package VASP[19]. Core electrons are replaced by ultrasoft pseudopotentials within the projector augmented wave (PAW) method[20,21]

and the $2p$ and $2s$ electrons for boron, nitrogen and oxygen are treated as valence electrons. The generalized gradient approximation (GGA) as formulated by Perdew-Burke-Ernzerhof[22] is employed for the exchange-correlation energy. A kinetic cutoff energy of 400 eV was used for the plane waves. For the non-defective bulk calculations a $4 \times 4 \times 2$ supercell with a total of 128 atoms was constructed and the Brillouin zone was sampled at the Γ point. For the defect calculations the supercell was increased to a $11 \times 11 \times 1$ for the bulk calculations to ensure the isolation of the defect from its periodic image. A $6 \times 6 \times 2$ cell with 10 Å of vacuum along the c-axis of the cell was used for the surface cell calculations. Van der Waals interactions were accounted for by applying the corrective scheme of Tkatchenko and Scheffler[23] as implemented in VASP. The supercell structures were optimized by minimizing the Hellmann-Feynman forces acting on the nuclei below the threshold value 0.02 eV Å^{-1}. Thermally induced structural distortions of the bulk h-BN crystal lattice were simulated by sampling the canonical ensemble (NVT) at a finite temperature of $T = 300$ K regulated by a Nosé-Hoover thermostat. The timestep of integration was set to 0.2 fs. The system was thermally equilibrated for 50 ps after which the micro canonical ensemble (NVE) was sampled for an additional 10 ps, maintaining a temperature of $T = 320$ K. From the last 10 ps of the simulated trajectory, 5 snapshots, each separated by 2 ps, were taken to represent a statistical average of the structure at finite temperature.

B. Formation energies

The formation energy E^f of a defect X in charge state q is commonly estimated by the equation[24]

$$E^f[X^q] = E[X^q] + E^q_{\text{corr}} - E[\text{host}] - \sum n_i \mu_i + q(\epsilon_F + \epsilon_v + \Delta v) \quad (1)$$

where $E[X^q]$ and $E[\text{host}]$ are the total energies of the defective and pristine host structures respectively as derived from supercell calculations. The amount of particles of type i, both native and impure, that are added or removed is given by n_i which is positive for a net amount of particles added and negative otherwise. The native and impurity atoms are assumed to be exchanged with a reservoir at a chemical potential given by μ_i. The chemical potentials for oxygen, nitrogen, hydrogen, and boron are computed from the Gibbs free energy from an O_2, N_2 and H_2 molecule in the gas phase and rhombohedral boron in the solid phase, respectively. The charge state q is included explicitly in the last term and describes the cost of adding or removing electrons from a reservoir at a potential set by the Fermi energy ϵ_F referenced with respect to the energy of the valence band maximum ϵ_v of the bulk reference cell. In general, in charged supercell calculations, due to periodic boundary effects, the reference potentials in the bulk and the defective supercell structures are not equal and need to be aligned with a term Δv[25]. Additionally, an image-charge correction term E^q_{corr} has to be added to account for spurious long-range Coulomb interactions between the defect charge, its periodic images and the neutralizing background charge[24].

C. X-ray absorption spectroscopy

X-ray absorption spectroscopy (XAS) was simulated within the DFT-XCH approach[26] where the photo excited atom is modeled by removing a core electron from the pseudopotential and placing it in the first available empty state. The electronic structure problem of the system that now includes the core-hole is then solved self-consistently under constrained occupations while employing the Shirley interpolation scheme[27] to generate optimal basis sets in order to reduce computational cost. The absorption spectrum is computed by evaluating the transition probability between the initial and final state as given by Fermi's golden rule within the dipole approximation. The resulting spectrum is broadened uniformly with a Gaussian of 0.2 eV at full width half maximum. To correct for the well-known underestimation of the band gap by the PBE functional, the energy scale is stretched uniformly by a factor of 1.04. Due to the lack of an absolute energy reference inherent in the pseudopotential method, an energy alignment scheme was employed to yield comparably meaningful relative energies for structurally and chemically different systems[28]. Finally the entire spectrum is shifted by a single value, that is kept constant for all computed spectra, to align with the experimental data.

II. RESULTS

A. Structure of triangular voids

To investigate the structural and thermodynamic stability of equilateral triangular defects in h-BN, we created periodic supercell models of defects with varying edge termination and size in a crystalline host. We considered defects in both bulk and surface slab supercells and defect sizes originating from just a single vacancy with 3 edge atoms up to a void created by removing 16 atoms yielding 12 edge atoms in total. In addition to the experimentally observed N- and B-terminated edges, we also investigate the possibility of oxygen terminated edges and defects with N- or B-terminated edges passivated with hydrogen atoms. Additionally we considered N-terminated defects with passivated dangling bonds by electron doping instead of hydrogen. A schematic representation of a subset of the relaxed supercells used in the calculations is displayed in Fig. 1.

All but the O-terminated defects suffered from a large distortion of the crystal lattice, especially in the vicin-

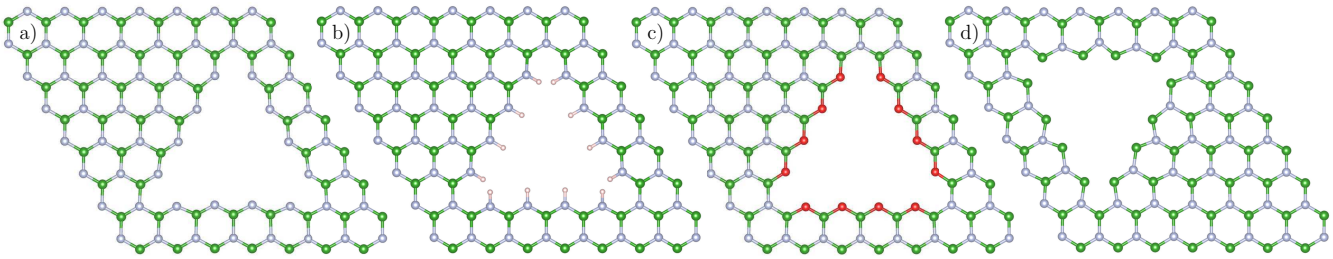

FIG. 1. (Color online) Partial images of h-BN crystalline supercell including triangular defect with four out of six different edge terminations investigated in this study: (a) electron doped nitrogen terminated $V^{N:e}_{B_{10}N_6}$, (b) hydrogen passivated nitrogen terminated $V^{N:H}_{B_{10}N_6}$, (c) oxygen terminated $V^{O}_{B_{10}N_6}$ and (d) boron terminated $V^{B}_{B_6N_{10}}$. The structures shown are all relaxed under neutral charge conditions with the exception of the nitrogen terminated case, where one electron was added for each under coordinated edge atom. Hydrogen, nitrogen, boron and oxygen atoms are colored pink, light blue, green and red respectively (or from lightest to dark grey in the same order).

ity of the created triangular void for all considered sizes. The distortion of the crystal lattice after relaxing the O-terminated defects was minimal with oxygen atoms displacing slightly away from the center of the void. In the case of B-terminated edges shown in Fig. 1 (d), the boron atoms at the edge of the void are undercoordinated and have a dangling bond which leads to the contraction of the void where the corners of the defect almost form a pentagon. Similar behavior is observed for the neutral N-terminated defects depicted in Fig. 2 (a), but the deformation is even stronger compared to B-terminated defects. By doping the N-terminated defect structures with additional electrons (one for each N edge atom) the dangling bonds are passivated and the triangular shape of the void is largely restored as seen in Fig. 2 (c). Doping the structure with electrons does however result in the deformation of the planar symmetry as shown in Fig. 2 (d). This planar deformation of the defective plane only occurs in the asymmetric surface slab calculation for a charged supercell and this effect was not observed in the neutral surface slab configuration as shown in Fig. 2 (b) nor in the charged bulk supercells. In the charged bulk supercells similar distorting effects are present but, mirrored symmetrically on both sides of the defective plane, these are canceled out.

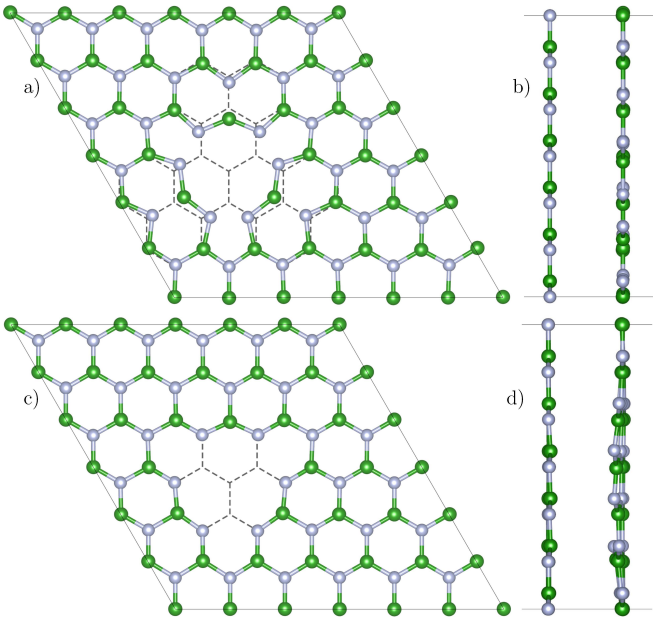

FIG. 2. (Color online) Top view of part of the surface plane of the $V^{N}_{B_3N_1}$ supercell model for the (a) neutral and (c) charged supercell surface slab model. The side views (b) and (d) correspond to the top two layers of the neutrally and negatively charged slab respectively, with the rightmost plane being the surface plane. The dashed lines indicate the unperturbed crystal lattice.

	Boron:H		Nitrogen:H	
Defect size	Average	Max	Average	Max
V_{B_1}	1.09	1.30	0.69	1.02
$V_{B_3N_1}$	0.95	1.12	0.59	0.72
$V_{B_6N_3}$	0.64	1.00	0.49	0.77
$V_{B_{10}N_6}$	0.65	0.98	0.47	0.79
V_{B_1}	1.08	1.09	0.83	1.35
$V_{B_3N_1}$	0.97	1.38	0.61	0.74

TABLE I. Average and maximum vertical planar displacement in Å of hydrogen atoms in hydrogen passivated B- and N-terminated defects.

Defect structures with B- and N-terminated edge passivated by hydrogen also showed significant structural deformation around the defect void. The hydrogen atoms in H-passivated defects (see Fig. 1 (b) in the case of the passivated N-terminated edge) are all oriented perpendicular with respect to their parent edge and, along with the nitrogen or boron atoms they bond to, undergo heavy buckling out of the crystalline plane. The average and maximum planar displacement of hydrogen atoms in H-passivated B- and N-terminated edges are presented in Table I. For the smaller defects the vertical displacement can be as much as 1.38 Ångstrom and as the defect

grows the average displacement seems to reach an equilibrium value. This can be understood from the fact that at a vertex of a triangular defect two passivating hydrogens atoms are at closest proximity in plane and therefore have to displace further out of plane to maintain the appropriate distance from each other. For the smallest defect all three passivating hydrogen atoms are at the triangles vertex but for increasing defect size hydrogen atoms appear that are on the triangle side. The boron terminated defects exhibited even stronger buckling compared to the N-terminated defects which is reflected by the larger average displacement of hydrogen atoms.

B. Triangular defect formation energy

The thermal stability of defects can be quantified by calculating the formation energies given by Eq. 1. Schemes to calculate the charge correction terms E^q_{corr} and $q\Delta v$ only exist for point-defects and not for multi-defect systems that we investigate in this work. Given that the electron doped N-terminated defects are the only charged cells and that the charge corrections become less prominent for increasing supercell sizes and the supercells used for these calculations are quite large, it is reasonable to neglect these corrections as we have done in our calculations. Computed formation energies for $\epsilon_F = 0$ in eV per edge atom for the various defect structures are shown in Table II. Note that the difference between surface and bulk formation energies is almost negligible within the accuracy of the calculations for almost all size and termination types. The most apparent conclusion that can be drawn instantly is that the O-terminated defects have the lowest formation energy and are therefore energetically most favorable for all defect sizes considered, which perfectly mirrors the minimal crystal distortion observed for O-terminated defects after relaxation as discussed in the previous section. The electron doped N-terminated defects have the largest formation energies closely followed by the unpassivated N- and B-terminated edges. As described in the previous section, the added electrons reduce the in-plane deformation but also cause an interaction with neighboring planes which in the asymmetric surface case leads to planar deformation (see Fig. 2). An increased Fermi level will reduce the formation energy for the electron passivated N-terminated defects but a value of $\epsilon_F = 7$ eV is required to approach the formation energies of the O-terminated defects which is larger than the material band gap and is highly unlikely to occur. Passivating the dangling bonds of the under coordinated edge atoms for B- and N-terminated defects with hydrogen atoms reduces the formation energy significantly but is still less favorable compared to the O-terminated defects. The difference in formation energies between hydrogen passivated and unpassivated defects is smaller for B-terminated defects compared to the N-terminated defects and can be explained by the fact that even though the addition of hydrogen passivates the dangling bonds and reduces the formation cost, this comes at the expense of planar deformation around the defect edge which is larger for B-terminated defects.

	Edge termination and/or passivation					
Defect size	B	B:H	N	N:H	N:e	O
V_{B_1}	2.48	1.78	3.33	0.91	5.83	−1.36
$V_{\text{B}_3\text{N}_1}$	2.26	1.79	3.26	1.13	6.23	−1.02
$V_{\text{B}_6\text{N}_3}$	3.16	2.06	3.88	1.39	6.49	−0.63
$V_{\text{B}_{10}\text{N}_6}$	3.81	2.38	4.39	1.76	6.59	−0.23
V_{B_1}	2.46	1.53	3.31	0.72	5.73	−1.33
$V_{\text{B}_3\text{N}_1}$	2.36	1.77	3.41	1.11	6.49	−0.95

TABLE II. Computed formation energies in eV per edge atom, for triangular defects in h-BN for different sizes with boron (B), nitrogen (N) or oxygen (O) terminated edges. Formation energies of defects with boron- and nitrogen terminated edges passivated by hydrogen are denoted by B:H and N:H respectively. The column marked N:e represents the formation energies of defects with nitrogen terminated edges with one doped electron per edge atom. The upper half of the table are computed values for defects in the bulk supercell whereas the lower half of the table represents defect formation energies in the surface layer of a slab supercell. The Fermi level with respect to the valence band maximum in the bulk was set to $\epsilon_F = 0$.

Defects that are created *in situ* during TEM measurements, due to the high energy electron beam, are likely to be N-terminated and, in agreement with our results, have been observed to be unstable[9,12]. Sample preparation methods that employ plasma to etch a multilayer down to a monolayer can introduce contaminants like oxygen into the sample prior to the measurement[11]. We find that, in contrast with the highly unstable N-terminated edges, O-terminated edges are very stable from a thermodynamic point of view and should be taken into account as a potential cause of triangular voids when studying defects in h-BN. To the best of our knowledge, O-terminated triangular voids in h-BN have not yet been considered in the TEM literature but, as mentioned in the introduction, the presence of oxygen defects in bulk or thin film h-BN has been proposed in several x-ray absorption spectroscopy studies[16–18].

C. XAS of hexagonal boron nitride

We have experimentally collected the boron K-edge absorption spectrum of a typical defective multilayer h-BN sample (see the appendix for experimental details), displayed as a dotted black line in Fig. 3 (a–b). The main feature at 192 eV is typical for pristine h-BN and originates from an excitonic state with π^* character located in the band gap. A visual representation of the wavefunction corresponding to this state is plotted in Fig. 3 (c–d) and its highly localized character explains the high inten-

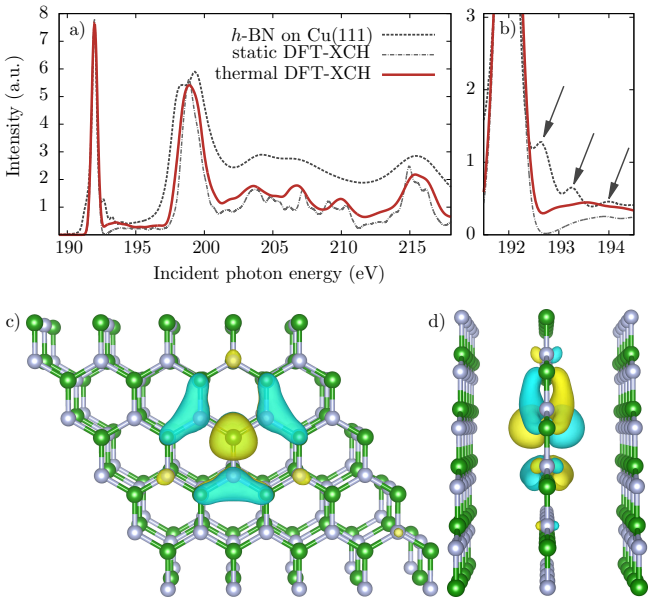

FIG. 3. (Color online) (a) Measured and simulated x-ray absorption spectrum of the boron K-edge in h-BN. The dotted black line is the measured spectrum for the 13 nm thin-film on Cu(111) substrate. The simulated spectra for the static structure at $T = 0$ K and the thermally equilibrated structure are shown in a dashed grey and solid red line respectively. (b) Close up of main π^* and three satellite features indicated by arrows. (c) Top and (d) side view of a $5 \times 5 \times 1$ h-BN supercell with an isosurface representation of the squared wavefunction $|\psi(\vec{r})|^2$ of the excitonic state corresponding to the intense transition in the B K-edge spectrum at 192 eV. The excitonic state is highly localized and has distinct antibonding p-like character.

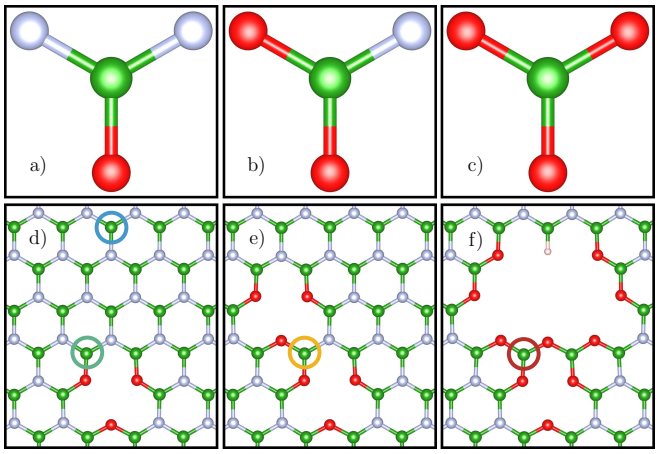

FIG. 4. (Color online) (a–c) Schematic representation of the $BN_{3-x}O_x$ $(1 \leq x \leq 3)$ substitutional oxygen defect environments of boron atoms in h-BN. (d–f) Defect structures in a h-BN host crystal, that host a boron atom with BN_2O, BNO_2 and BO_3 environment respectively, while maintaining twofold coordination for the oxygen atoms and threefold coordination for nitrogen and boron atoms. The circles around selected boron atoms color correspond to spectra in Fig. 5.

sity of the corresponding feature in the x-ray absorption spectrum. The three additional lower intensity features on the high energy side of the π^* observed in the spectrum of the defective thin film are experimentally not observed for pristine h-BN[15]. We have computed the x-ray absorption spectrum within the density functional theory framework for pristine h-BN at $T = 0$ and $T = 320$ K (shown in Fig. 3 (a–b) as the dashed grey and solid red line respectively) and the absence of the triplet of π^* transitions in either spectrum confirms that these transitions can not be associated with pristine h-BN nor by structural changes induced by thermal effects. The relative intensity of the triplet of π^* features with respect to the main π^* transition has been shown to be positively correlated with the total oxygen content of the film and therefore it has been hypothesized that the satellite peaks originate from boron atoms whose local BN_3 coordination is altered by the substitution of up to three nitrogen atoms with oxygen atoms, where the higher energy peak corresponds to a boron atom coordinated to three oxygen atoms[16–18]. A rigorous theoretical study on the direct effect of substitutional oxygen defects on the x-ray absorption spectrum of h-BN, however, has not yet been carried out.

D. Oxygen defects form triangular voids

To verify the proposed origin of the π^* satellites as a result of oxygen defects we first need to determine the structural model with which oxygen atoms are incorporated in the hexagonal boron nitride crystal lattice. Schematic representations of the three increasingly oxygen coordinated environments are shown in Fig. 4 (a–c) which will henceforth be referred to as BN_2O, BNO_2 and BO_3 respectively. Creating any one of these $BN_{3-x}O_x$ $(1 \leq x \leq 3)$ defect environments in a crystalline h-BN supercell, quickly reveals an issue with this structural model, proposed in previous experimental literature[16–18]. By simply replacing nitrogen with oxygen atoms, the oxygen atoms in the final defect structure will be over coordinated. The structure of the most stable crystalline boron oxide B_2O_3 reveals that unlike the trigonally bonded boron and nitrogen in h-BN, a twofold coordination is more favorable for oxygen. Attempts to relax the defect structures with trigonally coordinated oxygen atoms resulted in a strong distortion of the planar symmetry and for BO_3 the central boron atom was fully ejected out of the plane. This strongly reflects the tendency for the oxygen atoms to attain twofold coordination. To construct substitutional oxygen defects that yield $BN_{3-x}O_x$ local environments within the crystalline h-BN host, additional vacancies have to be created to ensure the twofold coordination of the oxygen atoms. Defective supercell structures that support each of the three local environments BN_2O, BNO_2 and BO_3 are shown in Fig. 4 (d–f),

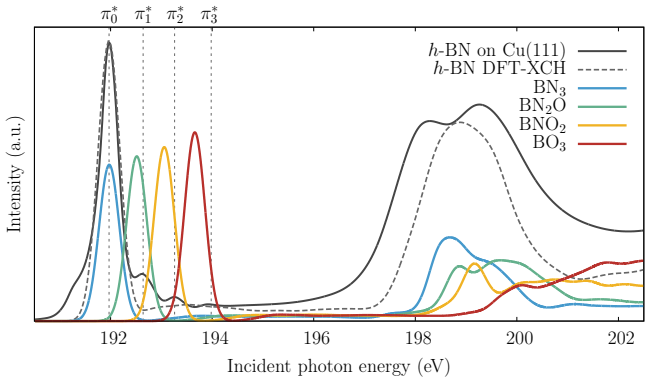

FIG. 5. (Color online) Measured and simulated B K-edge x-ray absorption spectra for hexagonal boron nitride. The solid black line corresponds to the measured spectrum for multilayer h-BN on a Cu(111) substrate and the dashed grey line is the thermally averaged simulation. The four colored spectra with the first peak increasing from lower to higher energy, represent the simulated spectrum of a single boron atom with a local BN_3, BN_2O, BNO_2 and BO_3 environment, respectively. The labels π_0^*–π_3^* and corresponding vertical dashed lines denote the energy position of the main π^* and satellite peaks as observed in experiment.

respectively. It is crucial to realize that this immediately reveals the intrinsic connection between oxygen defects and triangular voids in h-BN, as they form in parallel, directly as a result of the preferred coordination difference between oxygen and nitrogen.

E. XAS of oxygen defects in h-BN

Computed x-ray absorption spectra for excited boron atoms in each of the four possible oxygen coordination environments are shown in Fig. 5. The four features observed in the experimental spectrum, labeled π_0^*, π_1^*, π_2^* and π_3^* are hypothesized to correspond to excitations from boron atoms that have a local BN_3, BN_2O, BNO_2 and BO_3 local environment, respectively. In agreement with the hypothesis, the simulated spectra show an increasing blue shift of the main absorption feature for an increasing oxygen coordination of the boron atom. The blue shift arises due to two competing processes. Oxygen is more electronegative compared to nitrogen and so the partial charge on a boron atom will become more positive for an increasing oxygen coordination. An increase in the partial positive charge will reduce the possible screening of core-excitations, thereby deepening the core level binding energies, effectively increasing the energy separation between the 1s level and the first available empty state into which the core electron is excited. The oxygen defects also influence the density of states of the material, changing the relative energy separation of the unoccupied orbitals with respect to the core states. Unlike the screening of core states effect, this change in the unoccupied density of states does not necessarily have to result in a blue shift but could also cause a red shift. It is important to note that the character of the excitonic state does not change as the oxygen coordination of the excited boron atom changes and remains a highly localized state with anti-bonding p-character. The electron density is mostly located on the excited atom itself and the bonds between its first and second nearest neighbors (see Fig. 3 (c–d)). These bonds are broken when oxygen atoms are introduced and effectively the excitonic state becomes even more localized on the remaining bonds. This increased localization also increases the overlap with the 1s core state which explains the increase in intensity of the π^* feature for an increasing oxygen coordination.

	Local environment of excited atom			
	BN_3	BN_2O	BNO_2	BO_3
h-BN	+2.21	-	-	-
Cluster 1	+2.21	+2.24	-	-
Cluster 2	+2.21	+2.25	+2.30	-
Cluster 3	+2.21	+2.25	+2.30	+2.34

TABLE III. Average partial charges for core-hole excited boron atoms with varying local configuration in bulk h-BN and the three structures with substitutional oxygen defects. The labels Cluster 1 through 3 correspond to supercell structures as depicted in Fig. 4 (d-f) respectively.

III. DISCUSSION

To investigate the effect of the deepening of the core levels we have computed the local electron population on the boron atoms through Bader analysis[29] for the various possible oxygen coordinations as shown in Table III.
The Bader charge analysis confirms that indeed for an increasing oxygen coordination, the partial charge on the boron atom becomes more positive. As described before, this reduces the screening of core electrons which increases the energy separation between the 1s core level state and the LUMO, resulting in a blue shift of the π^* feature in the XAS. The dependency between the oxygen coordination of the boron atom and its computed Bader charge is perfectly linear within the accuracy of the calculations. The same linear dependence is observed in the position of the π^* transitions as a function of oxygen coordination, both in experiment and simulation, with the exception of the highest energy satellite peak in experiment. The measured energy separations between the first three peaks are very consistent at $\Delta E = 0.63$ eV but the separation between the two peaks highest in energy is significantly higher at $\Delta E = 0.75$ eV, in agreement with previous experimental work[15,16,18]. It is interesting to note that the increase in energy separation for the two higher energy peaks is not observed in our simulations and a potential cause might be that boron atoms with BO_3 coordination actually lose their planar geom-

etry inherited from the h-BN crystal structure and obtain a more three-dimensional orientation reminiscent of the crystalline structure found in B_2O_3. When a significant BO_3 peak is observed, the corresponding amount oxygen is more likely to be located in small B_2O_3 clusters rather than as substitutional defects in the h-BN lattice. X-ray absorption simulations of the crystalline B_2O_3 system (not shown) indeed show a π^* transition at 194.0 eV which overlaps exactly with observations from experiment[16,18]. The remaining underestimation of the computed blue shift can be attributed to the fact that the energy alignment scheme does not account for self-interaction errors introduced by the quasiparticle approach. The computed spectra are aligned by comparing the energy of the ground state to the excited system with the core-hole and the self-interaction energy of the photo excited electron depends is not corrected for.

IV. CONCLUSIONS

In conclusion, we have presented a theoretical estimate of the thermodynamic stability of triangular defects in h-BN as observed in multiple TEM studies for various edge terminations. Nitrogen terminated defects are highly unstable in agreement with experimental TEM literature and are slightly stabilized by injecting additional electrons to passivate any dangling bonds. Oxygen terminated edges are found to be the most stable edge termination of the types considered and we suggest that there is a large probability for the existence of stable triangular defects with O-terminated edges in h-BN. It should be noted that this does not necessarily imply that defects investigated in the experimental TEM literature as discussed in this work were in fact O-terminated. As these defects are created *in-situ* under influence of the high energy electron beam during the measurement, they are most likely natively terminated by boron or nitrogen. However this work does show that any work that studies defects in h-BN should consider the presence of oxygen defects as a significant possibility.

Additionally, we provide first-principle calculations of boron K-edge x-ray absorption spectra to confirm the hypothesis that a commonly observed triplet of π^* transitions in the experimental XAS of defective h-BN films is due to substitutional oxygen defects that decorate the excited boron atom[16–18]. As a photo excited boron atom is increasingly oxygen coordinated its core levels deepen and the strong π^* excitonic transition is increasingly blue shifted. The structural model that is solely capable of explaining the structural stability and the additional defect features observed in the spectroscopy is that of oxygen atoms replacing nitrogen atoms in the hexagonal crystal lattice with the stringent constraint that the oxygen atoms are twofold coordinated. The difference between the twofold coordination of the substitutional oxygen and the threefold coordination of the boron and nitrogen directly causes the formation of equilateral shaped voids in the direct vicinity of the oxygen defects. These simulations provide indirect proof that any h-BN film that exhibits the triplet of π^* features in the boron K-edge will have triangular voids with O-terminated defects. This can be verified by a STEM-EELS experiment that actively looks for the predicted spectral signature in the boron K-edge spectrum.

Insights into the nature of defects in h-BN as presented in this work will prove valuable in future work that aims to minimize defect concentrations. Additionally, the predicted exceptional stability of O-terminated triangular defects may enable novel applications of purposefully created defects as in for example nano sieves.

ACKNOWLEDGMENTS

This work is supported by NanoNextNL, a micro and nanotechnology programme of the Dutch Government and 130 partners. We acknowledge the support of the Center for X-ray Optics of Lawrence Berkeley Laboratory and the Industrial Focus Group XUV Optics at the MESA+ Institute for Nanotechnology at the University of Twente, notably the partners ASML, Carl Zeiss SMT GmbH and the Foundation FOM. All the computational work was performed at the Molecular Foundry which is supported by the Office of Science, Office of Basic Energy Sciences, of the U.S. Department of Energy under Contract No. DE-AC02-05CH11231.

Appendix: Experimental Details

All x-ray absorption spectroscopy measurements were carried out at beamline 6.3.2 of the Advanced Light Source (ALS) synchrotron at Lawrence Berkeley National Laboratory (LBNL). A detailed description and characterization of the beamline and measurement chamber can be found elsewhere[30,31]. X-ray absorption measurements of the boron K-edge were collected in total electron yield (TEY) mode, from commercially available samples (Graphene Supermarket) of CVD grown thin-films of h-BN on Cu(111) foil[8]. The p-polarized incident soft x-ray beam had an angle of incidence of 1.5° with respect to the sample surface normal. Energy calibration was performed by comparing to absolute absorption edges of Si and B filters installed at the beamline. The collected spectra have the dark current signal subtracted to account for the systematic error and noise in the collector electronics. Subsequently the spectra are normalized by a spectrum collected by a photodiode to account for the intensity fluctuations in the x-ray beam as a function of photon energy. Since TEY is a surface sensitive technique and the h-BN films were 13 nm thick, the resulting spectra did not have to be corrected for collected electrons originating from the copper substrate.

* shuber@lbl.gov

[1] C. Zhi, Y. Bando, C. Tang, H. Kuwahara, and D. Golberg, Adv. Mater. **21**, 2889 (2009).

[2] L. Song, L. Ci, H. Lu, P. B. Sorokin, C. Jin, J. Ni, A. G. Kvashnin, D. G. Kvashnin, J. Lou, B. I. Yakobson, and P. M. Ajayan, Nano Letters **10**, 3209 (2010).

[3] Y. Chen, J. Zou, S. J. Campbell, and G. Le Caer, Applied Physics Letters **84** (2004).

[4] A. Zunger, A. Katzir, and A. Halperin, Phys. Rev. B **13**, 5560 (1976).

[5] K. Watanabe, T. Taniguchi, and H. Kanda, Nat Mater **3**, 404 (2004).

[6] K. K. Kim, A. Hsu, X. Jia, S. M. Kim, Y. Shi, M. Hofmann, D. Nezich, J. F. Rodriguez-Nieva, M. Dresselhaus, T. Palacios, and J. Kong, Nano Letters **12**, 161 (2012).

[7] C. R. Dean, A. F. Young, I. Meric, C. Lee, L. Wang, S. Sorgenfrei, K. Watanabe, T. Taniguchi, P. Kim, K. L. Shepard, and J. Hone, Nature Nanotech **5**, 722 (2010).

[8] K. K. Kim, A. Hsu, X. Jia, S. M. Kim, Y. Shi, M. Dresselhaus, T. Palacios, and J. Kong, ACS Nano **6**, 8583 (2012).

[9] C. Jin, F. Lin, K. Suenaga, and S. Iijima, Phys. Rev. Lett. **102**, 195505 (2009).

[10] J. C. Meyer, A. Chuvilin, G. Algara-Siller, J. Biskupek, and U. Kaiser, Nano Letters **9**, 2683 (2009).

[11] N. Alem, R. Erni, C. Kisielowski, M. D. Rossell, W. Gannett, and A. Zettl, Phys. Rev. B **80**, 155425 (2009).

[12] K. Suenaga, H. Kobayashi, and M. Koshino, Phys. Rev. Lett. **108**, 075501 (2012).

[13] O. Cretu, Y.-C. Lin, M. Koshino, L. H. G. Tizei, Z. Liu, and K. Suenaga, Phys. Rev. Lett. **114**, 075502 (2015).

[14] S. Azevedo, J. R. Kaschny, C. M. C. de Castilho, and F. de Brito Mota, Nanotechnology **18**, 495707 (2007).

[15] I. Jiménez, A. F. Jankowski, L. J. Terminello, D. G. J. Sutherland, J. A. Carlisle, G. L. Doll, W. M. Tong, D. K. Shuh, and F. J. Himpsel, Phys. Rev. B **55**, 12025 (1997).

[16] M. Niibe, K. Miyamoto, T. Mitamura, and K. Mochiji, Journal of Vacuum Science & Technology A **28** (2010).

[17] I. Caretti and I. Jiménez, Journal of Applied Physics **110**, 023511 (2011).

[18] K. Simonov, N. Vinogradov, M. Ng, A. Vinogradov, N. Mårtensson, and A. Preobrajenski, Surface Science **606**, 564 (2012).

[19] G. Kresse and J. Furthmüller, Physical Review B **54**, 11169 (1996).

[20] P. E. Blöchl, Physical Review B **50**, 17953 (1994).

[21] G. Kresse and D. Joubert, Physical Review B **59**, 1758 (1999).

[22] J. P. Perdew, K. Burke, and M. Ernzerhof, Phys. Rev. Lett. **77**, 3865 (1996).

[23] A. Tkatchenko and M. Scheffler, Phys. Rev. Lett. **102**, 073005 (2009).

[24] H.-P. Komsa, T. T. Rantala, and A. Pasquarello, Physical Review B **86**, 045112 (2012).

[25] C. G. V. de Walle, J. Appl. Phys. **95**, 3851 (2004).

[26] D. Prendergast and G. Galli, Phys. Rev. Lett. **96**, 215502 (2006).

[27] E. L. Shirley, Physical Review B **54**, 16464 (1996).

[28] A. H. England, A. M. Duffin, C. P. Schwartz, J. S. Uejio, D. Prendergast, and R. J. Saykally, Chemical Physics Letters **514**, 187 (2011).

[29] W. Tang, E. Sanville, and G. Henkelman, Journal of Physics: Condensed Matter **21**, 084204 (2009).

[30] J. Underwood and E. Gullikson, Journal of Electron Spectroscopy and Related Phenomena **92**, 265 (1998).

[31] E. M. Gullikson, S. Mrowka, and B. B. Kaufmann, "Recent developments in euv reflectometry at the advanced light source," (2001).